

Control Designs for Critical-Contingency Responsible Grid-Following Inverters and Seamless Transitions To and From Grid-Forming Modes

Jaesang Park^{1,a}, Alireza Askarian^{1,b}, and Srinivasa Salapaka^{1,c}

Abstract—This article introduces two control frameworks: one for Grid-Following (GFL) inverters aiding Grid-Forming (GFM) inverters in voltage regulation during large contingency events and optimizing power transactions under normal conditions; and another for seamless transitions between grid-tied and grid-isolated setups, managing voltage transient characteristics. In microgrids, GFM inverters regulate voltage, while GFL inverters handle power transactions. The proposed GFL control detects abrupt load/generation changes, adjusting power transactions using local storage to support GFM inverters during contingencies. Additionally, a transition control ensures smooth GFL-GFM shifts, reducing power and voltage fluctuations. Simulation results validate improved voltage regulation during contingencies and enhanced power tracking during slow changes, alongside minimized transient overshoot.

I. INTRODUCTION

With increasing concern for climate change, global efforts have been made in recent years to reduce carbon emissions. To mitigate the pollution from fossil-based power generation and achieve lower carbon emissions, renewable energy sources (RES) such as solar, wind, and hydro are being integrated on a large scale into the power network. These RES, often supplemented with energy storage devices like batteries, are connected to the grid through DC/AC inverters. Currently, most inverters operate in grid-following (GFL) mode, where the grid controls voltage and frequency while the inverter supplies power. However, achieving high RES penetration with GFL inverters poses challenges.

In microgrids, especially when grid-isolated, sudden large power events like load or generational changes can strain voltage regulation, resulting in significant deviations from nominal values. Similar deviations happen in grid-tied setups due to factors such as weather disturbances and uncertainties in power production, which worsen with high penetration of RES. Conventional GFL-based inverter control designs lack robustness against these deviations, leaving grid viability solely on Grid-Forming (GFM) inverters. However, if GFM inverters are overwhelmed by sudden changes, cascading failures may lead to grid instability.

One explored approach [1] is Frequency-Watt (FW) control. Here, the inverter maintains a desired power set-point within a specific frequency range. However, if the frequency exceeds this range, the inverter follows a droop curve instead of the precise set-point. While this method enhances grid stability, it struggles in weak microgrids where frequency

control is lax, resulting in erratic power injection. Moreover, when the frequency drops below the nominal value, continuous power injection attempted by the inverter control design may not be sustainable over long intervals, posing operational challenges. In contrast, [2] introduces virtual inertia, simulating synchronous machine dynamics, where the energy stored in DC link capacitors to mechanical inertia in synchronous machines, aiming to emulate traditional power generation behaviors that enhance grid stability. While it excels in steady-state active power tracking and frequency support, it mainly focuses on the active power-to-frequency response, neglecting dynamics of reactive power and voltage.

Relevant studies, such as those by [3] and [4], explore control strategies transitioning GFL and GFM modes. Here inverter control is changed from GFL to GFM based on amplitude/frequency deviations from nominal values. While suitable for grid-tied operations with occasional deviations, in weaker microgrids, operating all inverters in GFM mode might not be efficient. Our proposed control design enables inverters to switch to GFM-like voltage regulation only during rapid load or generation changes, operating as GFL inverters during gradual changes. This assists full-time GFM inverters during extreme power fluctuations while providing commanded power, like maximum power point tracking, during stable periods.

We make use of algebraic structures in our control design to enable transitions between GFL and GFM modes; thus facilitating smooth transitions of microgrids between grid-tied and grid-isolated states. In the event of a main power grid anomaly, RES can disconnect and form a microgrid, preventing a complete blackout. Our transition capability ensures the grid-isolated microgrid includes a GFM inverter for regulating frequency and voltage, while allowing other GFL inverters to connect, ensuring the presence of a GFM inverter within the newly formed microgrid consistently. The proposed control retains the functional advantages and stability aspects of the control strategies developed in [4]. The main distinctive feature is that our control design enables smooth transitions while *ensuring* safe transient voltage characteristics. In contrast, the strategy in [4] does not guarantee transient characteristics during transitions. For instance, their methods may introduce sudden jumps in the controller output when switching modes, potentially causing grid instability. Using the proposed GFL inverter, we demonstrate about 44% reduction in the Rate of Change of Frequency (RoCof) during sudden load changes compared to using a conventional GFL inverter. Additionally, with the proposed smooth transition algorithm, during the transition from GFL to GFM, we

¹ Department of Mechanical Science and Engineering, University of Illinois at Urbana-Champaign, 61801 IL, USA
^ajaesang4@illinois.edu, ^baskaria2@illinois.edu, ^csalapaka@illinois.edu

demonstrate that we can achieve only 1% of overshoot in active power compared to the sudden transition and no overshoot in reactive power.

II. OVERVIEW OF THE CONVENTIONAL GFL AND GFM INVERTER

A. Modeling of Inverter connected to a grid

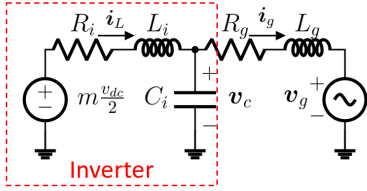


Fig. 1: The model of an inverter with LC filter connected to a grid.

A DC source power (e.g., RES) is transacted with an AC power grid using an inverter. An inverter with an LC filter connected to a grid can be modeled as in Fig. 1. It converts DC to AC using fast switching of transistors. A power converter (not shown here) takes power from the source and maintains a constant voltage V_{dc} at its output. The control design on the converter achieves voltage regulation by using capacitance or battery storage on the DC side. The inverter's switch-averaged model, depicted in Fig. 1, uses the modulating signal $m \in [-1, 1]$ as a control parameter. This signal is actuated using pulse-width modulated (PWM) signals, which determine duty cycles governing the switching. The averaged model resembles a controlled voltage source with output voltage $m \frac{V_{dc}}{2}$. However, to suppress high-frequency switching noise, an LC filter with resistance R_i , inductance L_i , and capacitance C_i is employed. This filter mitigates noise in the filter current i_L and the capacitor voltage V_c , which serves as the inverter's output voltage interfacing with the grid. The grid, represented as a voltage source with voltage V_g , is separated from the inverter by line impedance, modeled by line resistance R_g and inductance L_g . The output current i_g from the inverter is the power transacted with the grid.

B. Response of Conventional GFL to perturbation

The main goal of a GFL is to control its output power. Since the output power depends on the output current i_g and the capacitor voltage V_c , where V_c can be measured, its goal is converted to a controlling output current i_g .

Note that typically the control signal m is designed to make the inductor current i_L track $i_{L,ref}$, where the reference $i_{L,ref}$ is appropriately designed to make i_g track $i_{g,ref}$. In direct-quadrature (dq) coordinates, the dynamics between i_L and i_g is given by the capacitor dynamics as follows [5]

$$\hat{i}_g^{d,q} = \hat{i}_L^{d,q} - C_i \hat{V}_c^{d,q} s \pm C_i \omega \hat{V}_c^{q,d} \quad (1)$$

where superscript d and q respectively represent the direct and quadrature components, while the hat notation denotes the s-domain signal. Additionally, ω denotes the grid voltage frequency.

Here by choosing $\hat{i}_{L,ref}^{d,q} = \hat{i}_{g,ref}^{d,q} \mp C\omega \hat{V}_c^{q,q}$ and designing the filter current controller with a large bandwidth, the

coupling terms $C\omega V_c^d$ and $C\omega V_c^q$ cancel out and $\hat{i}_L^{d,q} \approx \hat{i}_{L,ref}^{d,q}$ resulting in the following dynamics given by

$$\hat{V}_c^{d,q} = \frac{1}{C_i s} (\hat{i}_{g,ref}^{d,q} - \hat{i}_g^{d,q}) \quad (2)$$

In addition to this, the frequency of the GFL control is determined by the PLL, which takes V_c^q as an input:

$$\hat{\omega} = K_{PLL}(s) \frac{1}{C_i s} (\hat{i}_{g,ref}^q - \hat{i}_g^q) + \hat{\omega}_0. \quad (3)$$

In this paper, we use subscript 0 to denote nominal values and superscript $-$ to represent amplitude of the underlying signals. Note that by assuming that the PLL accurately estimates the phase of the capacitance voltage, one can easily deduce from d - q transformations that $V_c^d \approx \hat{V}_c$ and $V_c^q \approx 0$. Also, it is easy to show that $P = \frac{3}{2}(V_c^d i_g^d + V_c^q i_g^q)$ and $Q = \frac{3}{2}(-V_c^d i_g^q + V_c^q i_g^d)$, i_g^d and i_g^q can be approximated as $i_g^d = \frac{2}{3V_0} P$, $i_{g,ref}^d = \frac{2}{3V_0} P_0$, $i_g^q = -\frac{2}{3V_0} Q$, and $i_{g,ref}^q = -\frac{2}{3V_0} Q_0$. See [5] for these d - q transformation details.

From (2) and (3), we obtain

$$\hat{V}_c = \frac{2}{3V_0 C_i s} (\hat{P} - P_0), \quad \hat{\omega} = \hat{\omega}_0 - \frac{2K_{PLL}(s)}{3V_0 C_i s} (\hat{Q} - Q_0). \quad (4)$$

Since the PI controller is widely used for $K_{PLL}(s)$, without loss of generality, both equations in (4) include at least one pure integrator. Therefore, they have infinite DC gain. Consequently, if there is a mismatch between the nominal output power and the actual output power, the GFL inverter cannot regulate voltage and frequency.

In addition, in (4), the nominal voltage V_0 is a grid parameter that we cannot change. Moreover, C_i is chosen to be small, just enough to reject the switching noise of a transistor, to minimize the effect of V_c on i_g . This makes the bandwidth of $\frac{2}{3V_0 C_i s}$ large. Therefore, a high-frequency disturbance in output power propagates to the inverter voltage and frequency, potentially leading to grid instability.

Some literature, like [6], proposes a GFL design that considers the bandwidth between active/reactive power and voltage/frequency. However, in most conventional designs, as mentioned earlier, this bandwidth is not adequately considered. Typically, only the bandwidth of the current controller and PLL are taken into account. Consequently, the bandwidth of (4) unintentionally becomes large, as noted.

C. Response of GFM to perturbation

Unlike GFL, the goal of GFM is to control the output voltage V_c . The corresponding control designs typically accommodate uncertainties in power generation and consumption, which translate into mismatches between the commanded and actual power transactions. Since physically it is impossible to accommodate these power mismatches without compromising the voltage (amplitude and frequency) regulation, the control laws allow the amplitude and frequency to *droop* or deviate from the nominal values; however, in a controlled manner.

There are several types of droop control strategies depending on the types of output line impedance. However, even though the line impedance could vary in type, in most cases,

it is inductive due to the presence of long transmission lines. Therefore, for simplicity, we assume a purely inductive line, and its droop strategy becomes the $Pf - QV$ type of droop [7], expressed as:

$$\hat{\omega} = \hat{\omega}_0 + K_P(\hat{P}_0 - \hat{P}), \quad \hat{V}_{ref} = \hat{V}_0 + K_Q(\hat{Q}_0 - \hat{Q}). \quad (5)$$

Here, $K_P(s) = k_p \frac{\omega_{lpf}}{s + \omega_{lpf}}$, $K_Q(s) = k_q \frac{\omega_{lpf}}{s + \omega_{lpf}}$, and k_p and k_q are the slope of the curve, while $\frac{\omega_{lpf}}{s + \omega_{lpf}}$ is a low pass filter for power calculation.

Both dynamics given in (5) have a finite dc-gain as they have no pole at the origin. Furthermore, k_p , k_q , and ω_{lpf} are design parameters, and by changing them, we can make the frequency and voltage insensitive to high-frequency disturbances of the output power. Therefore, even if there is a mismatch in nominal and actual output power, they can regulate the frequency and the magnitude of the voltage.

Therefore, when there are GFM inverters and conventional GFL inverters in the grid, when there is a disturbance of power, conventional GFL inverters do not contribute to voltage stability, and only GFM inverters respond to power mismatches and ensure a corresponding modified setpoint. However, in a network that has many GFL inverters, substantial and sudden power mismatches can overwhelm GFM inverters, thus compromising network stability. This motivates control designs where GFL inverters are more responsive to power uncertainties.

Remark: The power-grid network robustness discussed above is also referred to as inertia in some existing literature such as [2] and [8], where intuition is developed by developing analogies with a synchronous generator used in well-studied power plants. Here, we establish this connection in the context of our analysis. In a synchronous machine, the mechanical rotor acts as an energy storage device, the energy stored in the rotor being given by $E = \frac{1}{2}J\omega^2$, where J is the rotor moment of inertia, and ω is the rotating speed. Therefore, the rotor provides a mechanical means of absorbing or providing instantaneous power and prevents sudden changes in the rotating frequency of a synchronous machine. The swing equation and governor equations in (6) capture the dynamical behavior of the rotor frequency

$$J \frac{d\omega}{dt} = T_{in} - T_{out} - D\omega, \quad T_{in} = T_0 + k_\omega(\omega_0 - \omega), \quad (6)$$

where T_{in} is input torque comes from the governor, T_{out} is torque output due to electricity generation, and T_0 is nominal torque. Furthermore, D represents the damping of the rotor and k_ω is the governor droop coefficient. Using the approximation $P_0 = T_0\omega_0$ and $P = T_{out}\omega_0$, where P and P_0 are, respectively, the actual and nominal output power. Combining (6) together, as shown in [8], the dynamics of a synchronous generator can be expressed as

$$\hat{\omega} = \hat{\omega}_0 + \frac{1/H}{s + (k_\omega + D)/H}(\hat{P}_0 - \hat{P}), \quad (7)$$

where $H = J/\omega_0$. As shown in [9], by defining $\omega_{lpf} = (k_\omega + D)/J$ and $k_p = 1/(k_\omega + D)$, we can recover the first equation of (5). Also, as the mechanical inertia J

increases, the dynamics are less sensitive to changes in power. Therefore, inertia has an equivalent meaning in this context.

III. PROPOSED GFL CONTROLLER

We propose a control design in which the inverter responds to sudden and fast changes in power mismatches while being insensitive to slow changes. Here, we use our observations from the GFM droop-control design in the previous section, where we propose appropriately designing filters in the droop-control design to enable controllers that are sensitive to time constants of the load/generation perturbations. To be more specific, we will design controllers that mimic conventional GFL designs at low frequencies while mimicking the dynamics of (5) at frequencies higher than its cut-off frequency ω_{lpf} .

A. Power-injecting dynamics

The primary objective of GFL inverter is to control its output power. Designing such a controller using a droop-control structure requires analyzing the power-injecting dynamics. The droop equation relates output voltage amplitude and frequency to nominal and actual active/reactive power. However, these voltages and frequencies also impact active/reactive power. Illustrated in [10], this voltage-frequency-to-power relationship forms a feedback loop. Analyzing closed-loop power injection dynamics necessitates understanding power transaction dynamics. This relationship is given in the context of Fig 1, where the power transactions (P and Q) between the inverter output (specified by the output of the capacitor) and the point of coupling at the grid are given by $P + jQ = \bar{V}_c e^{j\theta_c} \left(\frac{\bar{V}_c e^{j\theta_c} - \bar{V}_g e^{j\theta_g}}{\bar{Z}_g e^{j\phi}} \right)^*$, where $\bar{Z}_g e^{j\phi} = R_g + j\omega L_g$ represents the line impedance. Assuming a long transmission line, we have $\phi \approx 90^\circ$. By linearizing this equation around $\theta_c - \theta_g = 0$ and $\bar{V}_g = V_0$, we obtain $\begin{bmatrix} P \\ Q \end{bmatrix} = \frac{V_0}{Z_g} \begin{bmatrix} 0 & 1 \\ 1 & 0 \end{bmatrix} \begin{bmatrix} \bar{V}_c - V_0 \\ V_0 \delta \end{bmatrix}$. In what follows, we assume that we have a voltage controller with a large bandwidth and therefore $\hat{V}_c = \hat{V}_{c,ref}$. Now we relate ω to δ by $\delta = \int_0^t (\omega - \omega_0) ds - \int_0^t (\omega_g - \omega_0) d\tau$. By combining (5) and using these relations, we derive the block diagram of closed-loop power injecting dynamics as shown in Fig. 2. Here, $\hat{d} = [\hat{V}_g - \hat{V}_0, \hat{\omega}_g - \hat{\omega}_0]^T$ and $\hat{p} = [\hat{P}, \hat{Q}]^T$ respectively represent amplitude and frequency deviations, and actual active and reactive power components.

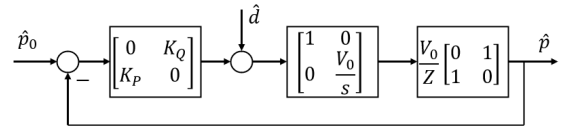


Fig. 2: Block diagram of droop-based power injecting dynamics

Since the dynamics from \hat{P}_0 to \hat{P} and the dynamics from \hat{Q}_0 to \hat{Q} are decoupled, they can be expressed as two Single-

Input Single-Output (SISO) systems as

$$\hat{P} = \frac{V_0^2 K_P}{s\bar{Z}_g + V_0^2 K_P} \hat{P}_0 + \frac{V_0^2}{s\bar{Z}_g + V_0^2 K_P} (\hat{\omega}_g - \hat{\omega}_0), \quad (8)$$

$$\hat{Q} = \frac{V_0 K_Q}{\bar{Z}_g + V_0 K_Q} \hat{Q}_0 + \frac{V_0}{\bar{Z}_g + V_0 K_Q} (\hat{V}_g - \hat{V}_0). \quad (9)$$

B. Design of the controller

For our control design, we consider the following criteria

1) *Reference tracking*: First, as discussed in the previous section, the goal of the GFL inverter is power tracking. At the very least, this should achieve steady-state power tracking. In frequency domain, it is equivalent to $\frac{\hat{p}(j0)}{\hat{p}_0(j0)} \approx I$ and $\frac{\hat{d}(j0)}{\hat{d}(j0)} \approx 0$. To achieve this, we propose the following control structure for $[K_P, K_Q] =$:

$$\left[\left(k_{p,P} + \frac{k_{i,P}}{s + \epsilon_P} \right), \left(k_{p,Q} + \frac{k_{i,Q}}{s + \epsilon_Q} \right) \right] \left(\frac{\omega_{lpf}}{s + \omega_{lpf}} \right). \quad (10)$$

Note that setting $\epsilon_P = \epsilon_Q = 0$ achieves $\frac{h(j0)}{h_0(j0)} = I$ and $\frac{h(j0)}{d(j0)} = 0$. Additionally, by choosing $\epsilon_P, \epsilon_Q > 0$, one can introduce robustness as a trade-off between performance. Finally, ϵ_P and ϵ_Q will be used in transition between GFL and GFM, a topic we will discuss later.

2) *Stability*: With the controller given in (10), the closed-loop characteristic polynomial for the system in (8) is $s^3 + (\omega_{lpf} + \epsilon_P)s^2 + (\omega_{lpf}\epsilon_P + \frac{V_g^2}{Z_g}\omega_{lpf}k_{p,P})s + \frac{V_g^2}{Z_g}\omega_{lpf}(k_{p,P}\epsilon_P + k_{i,P})$. Then, from the Routh-Hurwitz stability criterion if $\omega_{lpf} - k_{i,P}/k_{p,P} > 0$, it is stable. Also, for the second-order system in (9), since all the coefficients are positive, it stable for any $k_{p,Q}, k_{i,Q} > 0$.

3) *Robustness against a high-frequency perturbation*: Finally, among the controllers that meet the reference tracking and stability conditions mentioned above, our objective is to find the controller that mimics the response in (5) for $\omega > \omega_{lpf}$. With small ϵ_P, ϵ_Q , this can be achieved by setting $k_{i,P} = k_p$ and $k_{i,Q} = k_q$ while ensuring that $k_{i,P}/k_{p,P} \leq \omega_{lpf}$ and $k_{i,Q}/k_{p,Q} \leq \omega_{lpf}$.

IV. SMOOTH TRANSITION BETWEEN GFL AND GFM

Now we consider the implementation of control schemes that achieve transitions from GFL to GFM modes or vice versa, as desired. These transitions may be motivated by various reasons - for instance, decisions to go from grid-tied to grid-isolated modes. It turns out that we can achieve this by modifying parameters ϵ_P and ϵ_Q of our control design in (10). Specifically, when ϵ_P, ϵ_Q small, we obtain the GFL controller as previously designed. Conversely, selecting $\epsilon_P = \epsilon_Q = \epsilon_{max}$ for some large ϵ_{max} mimics a GFM defined in (5), as it derives $\frac{k_{i,P}}{s + \epsilon_P} \approx 0$ and $\frac{k_{i,Q}}{s + \epsilon_Q} \approx 0$.

A. Proposed transition strategy

1) *GFL to GFM*: The transition from GFL to GFM proposed in [4] is equivalent to change ϵ_P and ϵ_Q in (10) from 0 to ∞ abruptly. However, this abrupt change introduces a sudden variation in the control signal, potentially causing high-frequency perturbations in the grid and leading to grid instability. To mitigate this issue, we propose a smooth

transition method that gradually ramps up ϵ_P and ϵ_Q from 0 to ϵ_{max} .

2) *GFM to GFL*: On the other hand, when switching from GFM to GFL, even if we suddenly make ϵ to 0, the control signal does not experience abrupt changes. Therefore, to facilitate the transition from GFM to GFL, we use a jump from ϵ_{max} to 0.

B. Transition stability

First consider the transition stability of active power dynamics during the transition. As shown in the previous section, if a controller satisfies the stability conditions mentioned above, the system in (8) is stable for each $\epsilon_P \in [0, \epsilon_{max}]$. However, when ϵ_P varies, it becomes non-autonomous system and the stability of each time instance is not sufficient to guarantee overall stability.

Now, let $A_P(\epsilon_P)$ be the state matrix of a state space model of (8) corresponding to a given ϵ_P . Given that the system is stable for each ϵ_P , $A_P(\epsilon_P)$ is Hurwitz. Next, consider a solution to the Lyapunov equation $A_P^T(\epsilon_P)W_P(\epsilon_P) + W_P(\epsilon_P)A_P(\epsilon_P) = -I$. Since $A_P(\epsilon_P)$ is Hurwitz for each $\epsilon_P \in [0, \epsilon_{max}]$, the eigenvalues of $W_P(\epsilon_P)$ are all strictly positive. Finally, let $V_P(t) = x_P^T(t)W_P(\epsilon_P(t))x_P(t)$, where x_P is a state variable, be a Lyapunov candidate.

If there exists a finite $\alpha > 0$ such that $V_P(t) \leq \alpha V_P(0)$, then by Rayleigh Ritz theorem,

$$\|x_P(t)\|_2^2 \leq \alpha \frac{\max_{\epsilon_P \in [0, \epsilon_{max}]} \bar{\lambda}(W_P(\epsilon_P))}{\min_{\epsilon_P \in [0, \epsilon_{max}]} \underline{\lambda}(W_P(\epsilon_P))} \|x_P(0)\|_2^2. \quad (11)$$

Since the eigenvalues of $W_P(\epsilon)$ are strictly positive and $[0, \epsilon_{max}]$ is a closed interval, $\min_{\epsilon_P \in [0, \epsilon_{max}]} \underline{\lambda}(W_P(\epsilon_P)) > 0$, and the upper bound is finite. Therefore, for any $\epsilon > 0$, there exists $\delta > 0$ such that if $\|x_0\| \leq \delta$, $\|x(t)\| \leq \epsilon$ and therefore, the system is stable.

Proposition 1. *There exists a finite $\alpha > 0$ during the transition.*

Proof 1. By taking the derivative of the Lyapunov candidate function and applying Rayleigh Ritz theorem, we obtain

$$\dot{V}_P(t) \leq \bar{\lambda}(\dot{W}_P(\epsilon_P(t)) - I) \|x_P(t)\|_2^2 \leq q(t)V_P(t), \text{ where}$$

$$q(t) = \begin{cases} \frac{|\bar{\lambda}(\dot{W}_P(\epsilon_P(t)))|}{\min_{\epsilon_P \in [0, \epsilon_{max}]} \underline{\lambda}(W_P)} & \text{if } \dot{\epsilon}_P \neq 0 \\ -\frac{1}{\max_{\epsilon_P \in [0, \epsilon_{max}]} \bar{\lambda}(W_P)} & \text{if } \dot{\epsilon}_P = 0 \end{cases}$$

Note that during the transition $\dot{\epsilon}_P \neq 0$, and $\bar{\lambda}(\dot{W}_P(\epsilon_P(t)) - I) = \bar{\lambda}(\dot{W}_P(\epsilon_P(t))) - 1 \leq |\bar{\lambda}(\dot{W}_P(\epsilon_P(t)))|$. Conversely, when remaining in one mode, $\dot{\epsilon}_P = 0$ and $\dot{W}_P(t) = 0$ as $\dot{W}_P = \frac{\partial W_P}{\partial \epsilon_P} \dot{\epsilon}_P$. Then, $\bar{\lambda}(\dot{W}_P(\epsilon_P(t)) - I) = -1$

By applying Gronwall-Bellman inequality, we obtain $V_P(t) \leq V_P(0) \exp(\int_0^t q(\tau) d\tau)$, and it is bounded since

$$\begin{aligned} \int_0^t q(\tau) d\tau &\leq \frac{\max_{\epsilon_P \in [0, \epsilon_{max}]} \|\partial W_P(\epsilon_P)/\partial \epsilon_P\|}{\min_{\epsilon_P \in [0, \epsilon_{max}]} \underline{\lambda}(W_P)} \int_0^t |\dot{\epsilon}_P(t)| d\tau \\ &\leq \frac{\max_{\epsilon_P \in [0, \epsilon_{max}]} \|\partial W_P(\epsilon_P)/\partial \epsilon_P\|}{\min_{\epsilon_P \in [0, \epsilon_{max}]} \underline{\lambda}(W_P)} \epsilon_{max}, \end{aligned}$$

where we choose (and assume) a transition strategy where ϵ_P changes monotonically with time.

Proposition 2. $\max_{\epsilon_P \in [0, \epsilon_{max}]} \left\| \frac{\partial W_P(\epsilon_P)}{\partial \epsilon_P} \right\|$ is finite.

Proof 2. Since the coefficients of the characteristic polynomial (8) are affine with respect to ϵ_P ; therefore $A_P(\epsilon)$ is also affine; that is $A_P(\epsilon_P) = A_P(0) + \epsilon_P B_P$ for some B_P . Also $\frac{\partial}{\partial \epsilon_P} e^{A_P(\epsilon_P)\tau} = B_P \tau e^{A_P(\epsilon_P)\tau}$.

If we choose $\epsilon_P(t)$ to be a smooth function of t , and using $W_P = (e^{A_P^\top(\epsilon_P)\tau} e^{A_P(\epsilon_P)\tau})$, we get

$$\left\| \frac{\partial W_P}{\partial \epsilon_P} \right\| \leq 2 \|B_P\| \int_0^\infty \tau \left\| e^{A_P^\top(\epsilon_P)\tau} e^{A_P(\epsilon_P)\tau} \right\| d\tau,$$

where since $A_P(\epsilon_P)$ is Hurwitz, $\|e^{A_P^\top(\epsilon_P)\tau} e^{A_P(\epsilon_P)\tau}\| \leq e^{-\lambda_P \tau}$ for some $\lambda_P > 0$. As a result, it is bounded for each ϵ_P . Furthermore, since $[0, \epsilon_{max}]$ is a closed and bounded interval, $\max_{\epsilon_P \in [0, \epsilon_{max}]} \|\partial W_P / \partial \epsilon_P\|$ is bounded.

For multiple transitions, if there is a time gap of at least $\max_{\epsilon_P \in [0, \epsilon_{max}]} \bar{\lambda}(W_P) \frac{\max_{\epsilon_P \in [0, \epsilon_{max}]} \|\partial W_P(\epsilon_P) / \partial \epsilon_P\|}{\min_{\epsilon_P} \bar{\lambda}(W_P)} \epsilon_{max}$ between the end of one transition and the start of new transition, it ensures that $V_P(T) < V_P(0)$ where T is the time when the new transition start. Then, the same upper bound for $V(t)$ can be applied to the new transition, ensuring stability.

Similar procedures can be followed for analyzing the transition stability of reactive power dynamics.

V. SIMULATION RESULTS

Implementation: We designed the droop controller for the proposed GFL inverter under the assumption that we have a voltage controller with a large bandwidth. To design such a controller, let us first consider the dynamics of the LC filter of the inverter in Fig. 1. In dq coordinates, the dynamics of the LC filter are given as follows:

$$L_i \frac{d\hat{i}_L^{d,q}}{dt} = m^{d,q} \frac{V_{dc}}{2} \pm L_i \omega \hat{i}_L^{q,d} - V_c^{d,q} - R_i \hat{i}_L^{d,q} \quad (12)$$

Based on [5], with the current controller K_c and feedback linearizing control that cancels out the d and q coupling terms, the control input can be represented as follows

$$\hat{m}^{d,q} = \frac{K_c (\hat{i}_{L,ref}^{d,q} - \hat{i}_L^{d,q}) \mp L_i \omega_0 \hat{i}_L^{q,q} + \hat{V}_c^{d,q}}{V_{dc}/2}. \quad (13)$$

Then, $\hat{i}_L^{d,q} = T_c \hat{i}_{L,ref}^{d,q}$ where $T_c = \frac{K_c G_i}{1 + K_c G_i}$ and $G_i = \frac{1}{L_i s + R_i}$. On top of the current control in (13), by choosing $\hat{i}_{L,ref}$ as

$$\hat{i}_{L,ref}^{d,q} = K_v (\hat{V}_{c,ref}^{d,q} - \hat{V}_c^{d,q}) \mp C_i \omega_0 \hat{V}_c^{q,d} + \hat{i}_g^{d,q}, \quad (14)$$

one can achieve $\hat{V}_c^{d,q} = T_v \hat{V}_{c,ref}^{d,q}$, where $T_v = \frac{K_v T_c G_v}{1 + K_v T_c G_v}$ and $G_v = \frac{1}{C_i s}$.

In this experiment, controllers with the following structure are utilized:

$$K_c = \frac{L_i s + R_i}{\tau_c s}, \quad K_v = k_{p,V} + \frac{k_{i,V}}{s}, \quad (15)$$

where parameters τ_c , $k_{p,V}$, and $k_{i,V}$ are tuned to have enough bandwidth. Also, the conventional GFL that is used for comparison is using the same K_c .

The proposed controller and the conventional GFL were implemented and tested using the MATLAB Simscape toolbox with a step size of 0.05 s. The grid and inverter parameters used in the simulations are as follows: $R_i = 0.2\Omega$, $L_i = 3.3mH$, $C_i = 40\mu F$, $R_g = 0.1\Omega$, $L_g = 1.86mH$. Additionally, the nominal voltage and frequency are set to $V_0 = 391V$ and $f_0 = 60Hz$. The chosen controller parameters are $k_{p,P} = 0.2, \text{rad}/(\text{s} \cdot \text{kW})$, $k_{i,P} = 0.1\omega_{lpf} \cdot k_{p,P}$, $k_{p,Q} = 0.2 \text{ V/kVAR}$, and $k_{i,Q} = \omega_{lpf} \cdot k_{p,Q}$.

(a) Power Tracking: First, we evaluate the active and reactive power tracking of the proposed controller with filter cutoff frequencies (ω_{lpf}) set to $4\pi \text{ rad/s}$, $5\pi \text{ rad/s}$, and $20\pi \text{ rad/s}$. We assume that the inverter with the proposed controller is connected to a stiff grid with $\omega_g = \omega_0$ and $V_g = V_0$. As shown in Fig.3, at $t = 1$ second, the active power reference is changed from 10kW to 12kW, and at $t = 4$ second, the reactive power set point is changed from 0kVAR to 2kVAR. Similarly, at $t = 7$ seconds, the active power P_0 changes from 12kW to 8kW, and at $t = 10$ seconds, the reactive power Q_0 changes from 2kVAR to -1kVAR. The proposed controller achieves steady-state tracking just as conventional GFL.

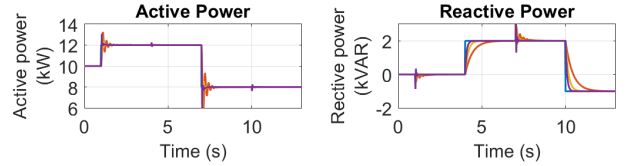


Fig. 3: Power reference (blue line) tracking of proposed GFL (red, orange, and purple line correspond to ω_{lpf} values of $4\pi \text{ rad/s}$, $10\pi \text{ rad/s}$, and $20\pi \text{ rad/s}$ respectively)

(b) Response to Fast and Slow Load Changes: For checking the frequency and voltage support of the proposed GFL, consider the case where the GFL inverter is connected to the GFM inverter, forming a weak microgrid. Initially, there is a 20kW active load and a 10kVAR reactive load, and the GFL inverter injects 10kW of active power. Throughout this scenario, $P_0 = 10kW$ and $Q_0 = 0V_{AR}$. At $t = 1s$, 5kW of active load and 5kVAR of reactive load are added to the grid. Then, the response is given as Fig.4

For conventional GFL, active and reactive output power converge to the reference value immediately. Then, a GFM inverter solely handles load changes and experiences a huge rate of change of frequency (RoCoF). However, with the proposed controller, in the event of a load change, the GFL inverter temporarily supplies power, resulting in smaller voltage and frequency peaks and reduced RoCoF until the grid reaches new steady-state values. When conventional GFL shows a RoCoF of 1.74 Hz/s, the proposed controllers with ω_{lpf} of 4π , 10π , and 20π achieve 0.89 Hz/s, 0.93 Hz/s, and 0.98 Hz/s, respectively, which represent 51.35%, 53.30%, and 56.00% of the RoCoF compared to the conventional GFL case. Additionally, the proposed GFL controller provides

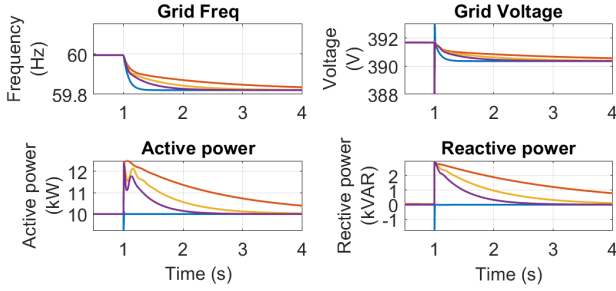


Fig. 4: Response against sudden load change with Conventional (blue line) and Proposed GFL (red, orange, and purple line correspond to ω_{lpf} values of 4π rad/s, 10π rad/s, and 20π rad/s respectively)

damping on the voltage.

Also, to verify that the proposed controller follows the power reference point and does not react to a slow load change, we apply 5 kW and 5 kVAR of active and reactive load changes over 5 seconds in a ramp manner to a microgrid with one GFM inverter and a proposed GFL inverter with $\omega_{lpf} = 20\pi$ rad/s. As seen in Fig. 5, when the load changes slowly, most of the load change is handled by the GFM inverter, and the GFL inverter with the proposed controller maintains its power reference point.

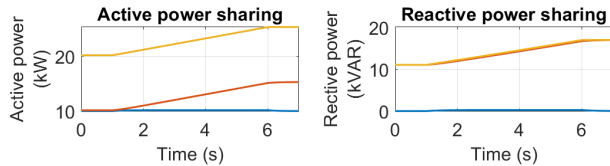


Fig. 5: Power sharing between GFM and proposed GFL under slow load change: Blue represents the proposed GFL, Red represents GFM, and Orange represents the total load.

(c) Transition between GFM and GFL: In the same microgrid setup with a GFL inverter utilizing the proposed controller ($\omega_{lpf} = 20\pi$ rad/s) and a GFM inverter, a transition between GFL and GFM is tested (Fig. 6). Initially, the proposed controller is in GFL mode. At $t = 2$ s, the GFL inverter transitions to GFM mode. Parameters $\epsilon = 100$ and $\epsilon_{max} = 200$ are chosen for smooth transition. For comparison, a sudden transition method proposed in [4] is also tested. Both methods exhibit stability, as shown in active and reactive power plots (Fig. 6). However, the smooth transition method demonstrates significantly lower overshoot and fluctuations compared to the sudden transition method. Specifically, during the transition, the sudden method results in a 4.1 kW active power overshoot, whereas the proposed method shows only 41 W . Similarly, the sudden method leads to a 4.4 kVAR reactive power overshoot, while the proposed method experiences none.

Furthermore, a transition from the GFM mode to the GFL mode is tested at $t = 7$ s. Here, for both methods, as explained before, ϵ_P and ϵ_Q jump from ϵ_{max} to 0. Even though the ϵ value changes abruptly from ϵ_{max} to 0, the transient is not significant because in GFL mode, control signals increases gradually and the transient is small.

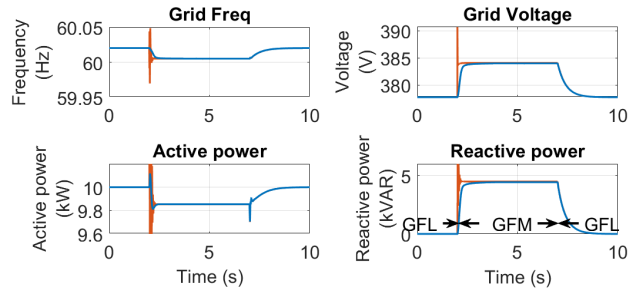


Fig. 6: Transition response between GFL and GFM mode: Blue represents proposed transition, Red represents sudden transition.

VI. CONCLUSIONS

In this paper, we evaluate the robustness of conventional GFL and GFM inverters against power perturbations by analyzing their power-to-voltage responses. We observe that conventional GFL exhibits sensitivity to perturbations, whereas the droop control structure in GFM enables shaping of this sensitivity. Motivated by this, we propose a GFL control structure that is insensitive to high-frequency load perturbations and tracks low-frequency power references. Furthermore, drawing on the structural similarity between the proposed GFL controller and the GFM controller, we devise a smooth transition strategy between GFL and GFM modes. This strategy minimizes power overshoot and oscillation during the transition.

REFERENCES

- [1] M. Elkhatib, J. Neely, and J. Johnson, "Evaluation of fast-frequency support functions in high penetration isolated power systems," in *2017 IEEE 44th Photovoltaic Specialist Conference (PVSC)*. IEEE, 2017, pp. 2141–2146.
- [2] Y. Qi, H. Deng, X. Liu, and Y. Tang, "Synthetic inertia control of grid-connected inverter considering the synchronization dynamics," *IEEE Transactions on Power Electronics*, vol. 37, no. 2, pp. 1411–1421, 2021.
- [3] J. Wang and G. Saraswat, "Study of inverter control strategies on the stability of low-inertia microgrid systems," in *IECON 2022–48th Annual Conference of the IEEE Industrial Electronics Society*. IEEE, 2022, pp. 1–6.
- [4] S. Chakraborty, S. Patel, G. Saraswat, A. Maqsood, and M. V. Salapaka, "Seamless transition of critical infrastructures using droop controlled grid-forming inverters," *IEEE Transactions on Industrial Electronics*, 2023.
- [5] A. Yazdani and R. Iravani, *Voltage-sourced converters in power systems: modeling, control, and applications*. John Wiley & Sons, 2010.
- [6] A. Askarian, J. Park, and S. Salapaka, "Enhanced grid following inverter (e-gfl): A unified control framework for stiff and weak grids," *IEEE Transactions on Power Electronics*, 2024.
- [7] Q.-C. Zhong and Y. Zeng, "Universal droop control of inverters with different types of output impedance," *IEEE access*, vol. 4, pp. 702–712, 2016.
- [8] J. Driesen and K. Visscher, "Virtual synchronous generators," in *2008 IEEE power and energy society general meeting-conversion and delivery of electrical energy in the 21st century*. IEEE, 2008, pp. 1–3.
- [9] J. Liu, Y. Miura, and T. Ise, "Comparison of dynamic characteristics between virtual synchronous generator and droop control in inverter-based distributed generators," *IEEE Transactions on Power Electronics*, vol. 31, no. 5, pp. 3600–3611, 2015.
- [10] A. Askarian, J. Park, and S. Salapaka, "Control design for inverters: Beyond steady-state droop laws," *arXiv preprint arXiv:2105.02292*, 2021.